Continuum constitutive models from analytical free energies

2007 J. Phys.: Condens. Matter 19 326207

(http://iopscience.iop.org/0953-8984/19/32/326207)

IOP PUBLISHING JOURNAL OF PHYSICS: CONDENSED MATTER

J. Phys.: Condens. Matter **19** (2007) 326207 (16pp) doi:10.1088/0953-8984/19/32/326207

Continuum constitutive models from analytical free energies

C J Kimmer and R E Jones

Sandia National Laboratories, Livermore, CA 94551-0969, USA

E-mail: cjkimme@sandia.gov

Received 14 March 2007, in final form 4 June 2007
Published 16 July 2007
Online at stacks.iop.org/JPhysCM/19/326207

Abstract

We present a critical investigation of the validity of the harmonic approximation for developing constitutive models for multiscale simulations. We examine models using the Cauchy–Born hypothesis within the quasiharmonic, local harmonic, and modified local harmonic approximations in order to characterize the strain and temperature dependence of the Cauchy stress for uniaxial, equibiaxial, and equitriaxial deformations. We compare these predictions with molecular dynamics simulations to evaluate the suitability of each harmonic model over a wide range of strains and temperatures. The various harmonic approximations are found to be very robust over a large temperature range. All the approximations make very similar predictions at small strains and temperatures. At larger strains and temperatures, the quasiharmonic model is the most accurate but also the most computationally expensive. The modified local harmonic model is seen to provide an accurate alternative to the full quasiharmonic model over a wide range of strains while being much less computationally expensive. The local harmonic model is similar in absolute accuracy to the modified local harmonic model, but the modified harmonic model is seen to more accurately predict the elastic moduli.

1. Introduction

Knowledge of the free energy of a system is crucial for understanding its properties as a function of temperature, stress, or strain. Although quite general numerical methods exist for computing the free energy of a system, many important problems only benefit from having analytical expressions for the free energy. For a crystalline solid, exact analytic expressions are available only if the interatomic interactions are linear so that the solid is harmonic. At low temperatures in a nonlinear solid, anharmonic effects may be small, and consequently the harmonic free energy can be an accurate and useful analytical approximation. Since anharmonic effects in a strained lattice can render the harmonic approximation invalid even at low temperatures, a

variety of approximations based on expanding the potential energy about the strained state have been developed.

The quasiharmonic (QH) approximation [1] is based on a second-order expansion about a homogeneously deformed reference state. The dynamics of the solid are approximated as harmonic oscillations around strained atomic positions which are expected to coincide with the average system configuration. The QH vibrational frequencies are found from the eigenvalues of the $3N \times 3N$ dynamical matrix. In contrast, the local harmonic (LH) approximation [2] neglects the vibrational coupling between atoms, and the vibrational frequencies are found from an approximate dynamical matrix that is only 3×3. A third approach, the so-called modified local harmonic model (MLH) [3] adds correction terms to the LH free energy in order to more closely approximate the QH free energy. The MLH approach yields a power series that is in principle exact for systems and strains that are sufficiently symmetric, but approximations are required in order to develop expressions for more general systems or strain states. In this paper, we present one such approximation developed in terms of an average local harmonic frequency which is suitable for anisotropic strain states and general crystal symmetries. The LH and MLH methods are less accurate than the QH model, but they have tremendous advantages in computational time even for moderately sized systems, due to the smaller dynamical matrices required.

Numerous studies have compared the accuracy of the various harmonic approximations for perfect crystals [4, 5, 2, 6] as well as systems containing grain boundaries and vacancies [6] or point defects [7]. Likewise, the QH models alone have been compared directly with molecular dynamics (MD) simulations for systems in an isotropic stress state [8]. Most of these studies focus on the accuracy of the free-energy function itself or the ability to predict the free energy associated with system inhomogeneities. Little attention has been paid to the validity of these harmonic models for systems in anisotropic stress or strain states. Likewise, while the pressure versus density or temperature has been extensively characterized, less attention has been paid to the accuracy of individual components of the stress tensor predicted by these models for more general stress or strain states.

A class of problems where the model's performance in general stress or strain states must be well understood is exemplified by current efforts to seamlessly couple MD and the finite element method (FEM) in a single, concurrent multiscale simulation. These simulations are expected to be accurate, efficient alternatives to current direct approaches for problems involving coupled physics with widely different characteristic length and time scales. A canonical example is brittle fracture and subsequent crack propagation. The fracture process ultimately depends on the rupture of individual bonds at or near the crack tip, yet the average deformation of atoms far from the crack tip is well characterized by the smooth continuum strain field of linear elasticity. Consequently, the region near the crack tip is modeled with MD while the longer-scale physics are modeled with FEM further from the crack. Among the currently proposed multiscale methods are the quasicontinuum method [9], the bridging-scale method [10], and coarse-grained molecular dynamics [11].

All these methods can at best match, in a locally averaged sense, the 'exact' solution obtained with a single MD simulation modeling the entire system. This constraint typically leads to an interpretation of the FEM region as a coarse-scaled atomic region with all atoms locally experiencing the same homogeneous deformation described by the continuum strain field. This interpretation, known as the Cauchy–Born (CB) hypothesis [12], allows the energetics of the continuum to be derived from the energy per unit volume of the homogeneously deforming atomic system. At nonzero temperature, the effects of thermal vibrations about the mean position are neglected in the continuum by the CB hypothesis. To include thermal effects in the coarse-scale constitutive model and to correctly couple to an

MD region at nonzero temperature, the CB hypothesis is extended so that only the ensemble-averaged deformation is homogeneous. Although not explicitly modeled, fluctuations about the average deformation contribute to the average stress tensor [13], so the long-time, large-scale dynamics modeled by the FEM region must correctly reproduce this average stress. Consequently, the continuum energetics and dynamics are obtained from the free energy, as in the finite-temperature CB methods [14, 15].

As mentioned earlier, most work has focused on the accuracy of the free energy function itself, while the MD–FEM coupling problem requires that the derivatives of the free energy with respect to the strain measure be accurate. Moreover, this accuracy must hold over a wide range of strains and deformations. The accuracy of these harmonic approximations has been previously examined as a function of volumetric strain [2, 4, 8], but such deformation represents only a small part of the full deformation space expected in a multiscale simulation. The reliability of these models for anisotropic deformation states has received much less attention.

Another issue that has received scant attention as it pertains to multiscale modeling is stability. A partial explanation for this lack of attention is because it is still not completely clear to those studying this field what the basic stability criteria for a stressed solid should be (see, e.g., [16–18], [19 chapters 5 and 6], [20 S.S. Antman's preface], and the references therein and also [21–26], which pertain specifically to crystals). This ambiguity arises, in part, because the criteria depend on the geometric description of the deformation of the stressed state [27] as well as on the thermodynamic mechanism maintaining the system in a constant stress ensemble [28]. For the multiscale problem, stability issues become important from the continuum viewpoint because the vanishing elastic moduli are equivalent to the loss of ellipticity of the equations of equilibrium. Moreover, implicit solution methods in FEM codes rely on the elastic moduli or their approximants in order to determine the continuum strain field. Stability analysis can consequently be seen as providing a bound on the strains and temperatures for which a coarse-scale stress model is valid.

We present a critical evaluation of the QH, LH, and MLH models for the specific purpose of deriving a temperature-dependent continuum constitutive model for a coupled MD–FEM simulation. We examine the effects of temperature as well as the type and amount of deformation on the average value of the stress tensor calculated from MD simulation. With these data, we investigate whether any of the existing harmonic approximations are valid over the range of temperatures and strains by comparing the data with predicted stress tensors of the various harmonic models. Finally, we point out that the differences observed between the various approximations have rather profound effects on stability estimates which may be important to the FEM application of the constitutive models. We find that the LH and QH models agree qualitatively only for the case of isotropic deformations. The QH and MLH models better capture the deformation dependence for all the anisotropic strain states considered here. Even though they are less accurate, the LH and MLH approaches may be preferred in practice because they are computationally inexpensive. For anisotropic models, the LH model performs worse than the MLH model. We show that this has implications for stability predictions using the LH model, so that the MLH model should be preferred over the LH model for multiscale methods as a reasonably accurate but less expensive alternative to the QH method.

The outline of the paper is as follows. In section 2 we present an overview of continuum stress tensors derived from the Helmholtz free energy using harmonic approximations. In section 2, we also present a general version of the MLH model suitable for anisotropic strains and any crystallographic symmetry. In section 3, we compare the harmonic predictions with MD simulation, and we conclude in section 4. In the appendix, we present useful expressions for implementing the various harmonic models and performing stability calculations.

2. Methodology

We consider a monatomic crystal in its reference state with atoms located at $\mathbf{R}^\alpha$ and labeled by their unit cell α. In particular, for an N-atom crystal we have $\sum_\alpha 1 = N$. A homogeneous deformation of the crystal maps any point $\mathbf{X}$ in the reference configuration to a point $\mathbf{x}$ in the strained configuration, and consequently atoms at $\mathbf{R}^\alpha$ map to $\mathbf{r}^\alpha = \mathsf{F} \cdot \mathbf{R}^\alpha$. Here F is the deformation gradient

$$\mathsf{F} \equiv \frac{\partial \mathbf{x}(\mathbf{X})}{\partial \mathbf{X}}. \tag{1}$$

The homogeneous deformation is viewed as describing the thermally averaged atomic positions so that the appropriate dynamic variables are the displacements $\mathbf{u}^\alpha$ measured *relative to the homogeneously deformed crystal*, i.e. the configuration represented by $\mathbf{r}^\alpha$. In an MD–FEM multiscale simulation, the displacements $\mathbf{u}^\alpha$ would be resolved at the FEM scale only in a thermally averaged sense while the longer wavelength degrees of freedom $\mathbf{r}^\alpha$ would be resolved fully. For simplicity, we restrict attention to interatomic potential energies Φ that are sums over pair potentials $\phi(r)$, but the treatment of more general cases is straightforward. In this case, the potential energy is given by

$$\Phi(\{\mathbf{u}^\alpha\}; \mathsf{F}) = \sum_{\alpha<\beta} \phi(\mathbf{r}^{\alpha\beta} + \mathbf{u}^{\alpha\beta}) \tag{2}$$

with $\mathbf{r}^{\alpha\beta} = \mathbf{r}^\alpha - \mathbf{r}^\beta$ and a similar definition for $\mathbf{u}^{\alpha\beta}$. At constant energy, the dynamics are derived from the Hamiltonian $\mathcal{H}$. At constant temperature T, the Helmholtz free energy $\mathcal{F}$ provides information about the system's static and dynamic properties. $\mathcal{F}$ is a function of F and T and a functional of Φ over the configurational space $\{\mathbf{u}^\alpha\}$. The first Piola–Kirchoff stress P is work-conjugate to F, namely

$$\mathsf{P} = V_0^{-1} \left.\frac{\partial \mathcal{F}}{\partial \mathsf{F}}\right|_T \tag{3}$$

where V_0 is the volume of the undeformed system. For comparison with MD simulation, the Cauchy stress, σ, may be equated with the time-averaged virial stress tensor [29] and the stress controlled by typical MD barostats [30]. The Cauchy stress is found from P

$$\sigma = J^{-1} \mathsf{P} \mathsf{F}^{\mathrm{T}} \tag{4}$$

where $J = \det \mathsf{F} = V/V_0$.

All the harmonic approximations studied here may be viewed as arising from an approximate Hamiltonian that depends on the deformation F but is quadratic in the atomic displacements. Within this approximation, $\mathcal{F}$ becomes the sum of the potential energy due to the average homogeneous deformation and a harmonic vibrational energy term. Omission of the vibrational energy term yields the familiar CB energetics and constitutive model for the averaged kinematics $\mathbf{r}^\alpha$. The vibrational terms describe uncoupled harmonic oscillators with frequencies $\{\omega_\gamma\}$. The actual values of the frequencies depend on the exact nature of the approximation used and will be treated shortly. To compare with MD, which is a classical simulation technique, we restrict attention to the classical or high-temperature limit ($\hbar\omega_\gamma \ll k_{\mathrm{B}}T$) where the distribution function obeys Boltzmann statistics. The free energy in the various harmonic models is then completely determined by the CB energy and the vibrational spectrum of the model [31]

$$\mathcal{F}(\mathsf{F}, T) = \Phi(\mathsf{F}) + k_{\mathrm{B}}T \sum_\gamma \ln\left(\frac{\hbar\omega_\gamma(\mathsf{F})}{k_{\mathrm{B}}T}\right). \tag{5}$$

The first term on the right-hand side is independent of temperature and is the energy of the CB system, $\mathcal{F}_{\rm CB} \equiv \Phi(\mathsf{F})$. The temperature dependence is determined by the vibrational spectrum in the second term above which we denote $\mathcal{F}_\omega$. Using (3), the first Piola–Kirchoff stress follows

$$V_0\mathsf{P} = \frac{\partial \Phi}{\partial \mathsf{F}} + k_{\rm B}T \sum_\gamma \omega_\gamma^{-1} \frac{\partial \omega_\gamma}{\partial \mathsf{F}} \tag{6}$$

where we have suppressed the dependence of the stress tensor on F and T for brevity. The first term on the right-hand side is the stress determined from the CB model, $V_0\mathsf{P}_{\rm CB} = \frac{\partial}{\partial \mathsf{F}}\mathcal{F}_{\rm CB}$. The temperature dependence of the constitutive model is solely due to the change in frequency with deformation which is a consequence of the anharmonicity of the potential. We denote these temperature dependent terms by P_ω. Thus, we have

$$\mathsf{P} = \mathsf{P}_{\rm CB} + \mathsf{P}_\omega \tag{7}$$

and may use an analogous decomposition and notation for the Cauchy stress tensor. This decomposition is advantageous since we consider the QH, LH, and MLH harmonic approximations which share the same CB term but differ in their treatment of the vibrational free energy and P_ω. Consequently, we use $\mathcal{F}_\omega$ only for the generic vibrational free energy term computed using any approximation and use $\mathcal{F}_{\rm QH}$, $\mathcal{F}_{\rm LH}$, and $\mathcal{F}_{\rm MLH}$ to refer to the vibrational free energy using one of the three specific harmonic approximations. A similar notation may be employed for the vibrational contributions to the stress calculated with each specific model. Finally, as seen from equation (6), P_ω is linear in temperature. This linearity is important in providing a means to ascertain whether *any* harmonic approximation is accurate in describing the thermally averaged dynamics over a given range.

Although each of the three different harmonic approximations differ in their treatment of the vibrational spectrum, they all depend fundamentally on the force constant matrix $D^{\alpha\beta} \equiv \frac{\partial^2}{\partial \mathbf{u}^\alpha \partial \mathbf{u}^\beta}\Phi$ describing the linear interaction of atom α with atom β. For defect-free crystals, translational invariance allows us to restrict attention to a subset of force-constant matrices $D^\alpha \equiv \frac{\partial^2}{\partial \mathbf{u}^\alpha \partial \mathbf{u}^0}\Phi$ for the bond between two atoms separated by $\mathbf{r}^\alpha$. The vibrational frequencies $\{\omega_\gamma\}$ in the QH approximation are determined from the eigenvalues $\omega^2_{\mathbf{K}\lambda}$ of the Fourier-transformed force constant matrix $D_{\rm QH}(\mathbf{K})$. This *dynamical matrix* is given by

$$D_{\rm QH}(\mathbf{K}) = \sum_\alpha D^\alpha \exp(-{\rm i}\mathbf{K}\cdot\mathbf{R}^\alpha). \tag{8}$$

The N wavevectors $\{\mathbf{K}\}$ span the lattice reciprocal to the *reference configuration*. The deformation of the reciprocal lattice need not be considered since $\mathbf{k}\cdot\mathbf{r}^\alpha = \mathbf{K}\cdot\mathbf{R}^\alpha$ is invariant under homogeneous deformation. The deformation dependence is contained in the force constant matrices and enters only through the derivatives of the potential evaluated in the strained configuration. The QH model for an N-atom monatomic crystal yields a maximum of N distinct wave-vectors $\mathbf{K}$ each corresponding to three frequency branches labeled by λ. The QH approximation thus models acoustic and optical branches as well as the dispersion relation for longitudinal and transverse normal modes.

In contrast to the QH model, the LH approximation neglects the coupling between interacting atoms. Each branch of the QH spectrum is then approximated by a single LH frequency. For a homogeneous monatomic system, the LH simplification of the QH model yields the single 3×3 dynamical matrix

$$D_{\rm LH} = \sum_\alpha D^\alpha \tag{9}$$

with three possibly degenerate eigenvalues ω^2_γ, $\gamma = 1, 2, 3$. Because of the drastic reduction in size of the dynamical matrices, the LH model is much less computationally expensive than

the QH model. The MLH model is likewise less expensive than the QH model, and it takes the form of a correction to the LH vibrational free energy. This correction is derived from the construction of an explicit expression for the difference between the QH free energy and the LH free energy [3]. For certain deformations where the local harmonic frequency is triply degenerate, this difference may be written exactly as a power series in the complete $3N \times 3N$ QH dynamical matrix. For more general deformations, we develop the MLH approximation in terms of an average frequency $\omega^6_{\mathrm{MLH}} \equiv \det D_{\mathrm{LH}}$, recovering the original method for isotropic deformations of cubic systems. The vibrational free energy within the MLH model is then given by:

$$\mathcal{F}_{\mathrm{MLH}} = \mathcal{F}_{\mathrm{LH}} - \frac{3Nk_{\mathrm{B}}T}{\omega^4_{\mathrm{MLH}}} \sum_{\alpha} \mathrm{Tr}(\mathbf{D}^{\alpha})^2 + \mathrm{O}(\mathbf{D}^3). \tag{10}$$

For this version of the MLH model, we retain only this first correction term before truncating the expression. The leading term in this power series is a second-order term proportional to the square of the QH dynamical matrix. For the homogeneous systems studied here, the correction term can be written as a sum of the square of the elements of the force constant matrices. We defer further details of the exact computation of the MLH correction term and the various harmonic stress-tensor calculations to the appendix.

As the expressions in the appendix indicate, successive derivatives of the frequencies with respect to the deformation gradient lead to increasingly unwieldy expressions for the stress tensor (first derivative) and elastic modulus (second derivatives). Consequently, evaluating successive derivatives is increasingly computationally expensive. The relative expenses of the free energy, stress tensor, and elastic modulus are independent of the number of atoms N for a homogenous system. The derivative of a frequency with respect to the 3×3 components of the deformation gradient yields a stress tensor evaluation roughly an order of magnitude more expensive than the free energy evaluation. Similarly, evaluation of the modulus incurs another order of magnitude increase in computational time. For evaluation of the free energies, the LH and QH models require only the frequency spectrum while the MLH model also requires the trace of the dynamical matrix squared. This MLH correction introduces little additional expense for typical interatomic potentials since it reduces to a sum over atoms interacting with a specific, central atom. For this work, we find the MLH model is at worst a factor of 2 slower than the corresponding LH evaluation. The QH model is a factor of N more expensive than the other harmonic models due to the required diagonalization of a 3×3 dynamical matrix for each of the N wave-vectors. This QH penalty is not prohibitive for a one-time evaluation at a given strain state, but the multiscale problem requires less expensive approximations for even moderately large N, precisely because repeated evaluations at arbitrary deformations are needed. In practice, we observe that the stress tensor evaluation within the QH model is feasible on a typical workstation. The additional order of magnitude increase for the elastic moduli is found to render their repeated evaluation within the QH approximation prohibitively expensive.

3. Results

The analytical expressions for the Helmholtz free energy and its strain derivatives presented in the previous section can provide predictions for several averaged quantities which may be obtained from MD simulation. Here we compare the predictions of the various harmonic models for the pressure and the diagonal components of the Cauchy stress tensor with MD data. Herein, we consider only deformations in which the off-diagonal stress components are zero.

The MD simulation method has been described in detail elsewhere [30], but we briefly describe our technical approach. We integrate Hamilton's equations of motion with the velocity

Verlet algorithm and thermostat our system with a Nose–Hoover thermostat. We use a smooth Lennard-Jones interatomic potential cutoff after second nearest neighbors. The specific cutoff distance as a function of deformation depends on the strain state, since the number of neighbors within a cutoff distance can change as the stretch is increased or decreased. The interatomic pair potential is

$$\phi(r) = 4\epsilon\left[\left(\frac{\sigma}{r}\right)^{12} - \left(\frac{\sigma}{r}\right)^{6}\right]. \tag{11}$$

We use reduced units where mass m is 1, energy is in units of ϵ, length is in units of σ, and stress is in units of ϵ/σ^3. We use a timestep of $\Delta t = 10^{-3}\sqrt{m\sigma^2/\epsilon}$ for all MD simulations. For each strain state and temperature, we apply the homogeneous deformation to the unstrained crystal and to the periodic simulation box. Initial velocities are chosen for each prescribed temperature from a Gaussian distribution with zero center of mass momentum and the correct temperature achieved by scaling. The system is equilibrated in the initial state for 40 000 time steps and then spatial and temporal averages are calculated for the next 160 000 time steps. The NVT ensemble is sampled using a Nose–Hoover thermostat with a characteristic period of 400 timesteps. We have verified that our ensemble averages and results are independent of the particular sampling scheme used and the specific value chosen for the thermostat mass.

We simulate an FCC crystal in a cubic periodic simulation cell with eight cubic unit cells on each side, yielding $N = 2048$ atoms. We investigate three different deformation states: uniaxial deformation (straining the (100) direction), equibiaxial deformation (straining (100) and (010) equally), and isotropic deformation (a volumetric strain) as a function of temperature and strain. In other words, each type of deformation is characterized by a single parameter, i.e. uniaxial deformation by F_{11}, equibiaxial deformation by $F_{11} = F_{22}$, and isotropic deformation by $F_{11} = F_{22} = F_{33}$. We consider stretches from -5% to $+10\%$ ($F_{11} = 0.95$–1.1), investigating both tension and compression over a wide range. For each strain state, we model temperatures $k_{\mathrm{B}}T$ ranging from 0 to a maximum of 1.2ϵ. For many strain states, this maximum temperature is above the melt temperature, and the solid becomes unstable well before this maximum temperature is reached. We show only data for stable solids at each strain state and temperature. We choose the zero-temperature stress-free lattice as our reference configuration.

Stress–strain curves at constant temperature for this system computed from the various harmonic models in uniaxial tension are shown in figure 1. Up to strains of about 3%, the approximations are seen to be indistinguishable. At higher strains, they show markedly different behaviors with the QH model in between the extremes suggested by the LH and MLH models. The MLH correction term added to the LH model is thus seen as an over-correction to the actual QH stress–strain curve, but both the LH and MLH approximations have roughly the same absolute error with respect to the QH values. One can ignore the complex frequency and deformation dependence of each model and characterize the differences in each stress strain curve by the derivatives of the stress tensor with respect to deformation and with respect to temperature. From this viewpoint, the LH provides an over-estimation of the deformation derivative while the MLH and QH models are qualitatively similar. Because of the simple dependence on temperature within the harmonic approximations, the derivative of stress with respect to temperature is constant.

For the temperature range studied here, we observe a linear variation of pressure with temperature as shown in figure 2 for equibiaxial deformation. These data are representative of similar results seen for isotropic and uniaxial deformations. At small strains, the data agree well with the harmonic approximations throughout the large temperature range. The melt temperature of the Lennard-Jones FCC crystal at zero pressure is 0.65ϵ–0.68ϵ, depending on the range of the potential [32]. Consequently, the suppression of surface effects by the periodic

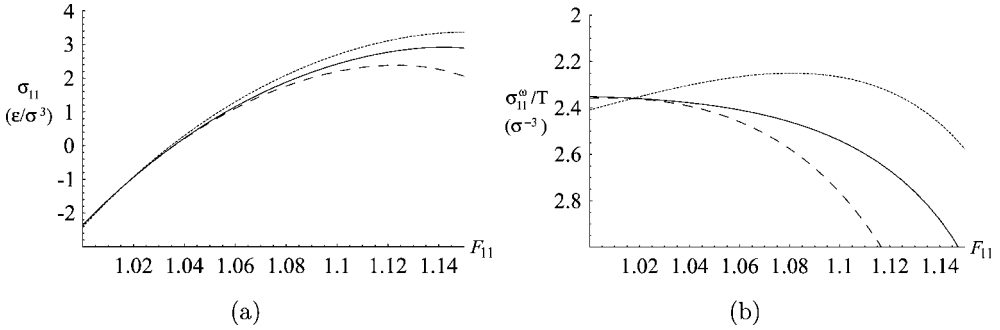

Figure 1. (a) Isothermal Cauchy stress–strain curves for $k_B T = \epsilon/4$ showing the predictions of the harmonic model for uniaxial tension. Shown is σ_{11} as predicted by the QH model (solid), the LH model (short dashes), and the MLH model (long dashes). The MLH model is seen to be an over-correction from the LH to the QH predictions. All models are virtually indistinguishable at small strains. (b) The frequency-dependent part of the stress scaled by temperature for the QH (solid), LH (long dashes), and MLH (short dashes) models.

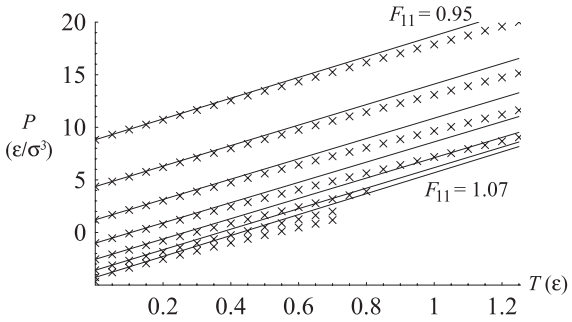

Figure 2. Comparison of the predicted LH pressure at constant deformation (solid lines) with the MD results (crosses) versus T for equibiaxial deformation over a range of strains and temperatures. The strain increases from top to bottom, and the LH approximation is seen to perform well at low temperatures and more poorly at high temperatures.

boundary conditions leads to some MD simulations being run for superheated Lennard-Jones crystals [33, 34]. Although the physical relevance of these simulations is scant, this large temperature range reveals that the predictions are reasonably close to the data even beyond the melt temperature. The harmonic approximations can be considered extremely robust even under the anisotropic deformations considered here. At higher stretches, the melting temperature is reduced. So, although the LH model performs more poorly at large temperatures and strains, it still performs well between zero temperature and the reduced melt temperature for each corresponding strain. It is also apparent that the LH approximation overestimates derivatives with respect to temperature. In fact, all three harmonic approximations are similar in this sense. The case of uniaxial deformation leads to the best agreement between simulation and the harmonic models, yet all three deformations studied clearly show deviations from the expected linear dependence. These deviations are small relative to the value of the pressure itself, so these harmonic approximations are indeed suitable over the temperature and strain ranges studied here.

The MD data display smooth variations in the energy or stress as a function of temperature and deformation up until critical strains or temperatures are reached. We associate the

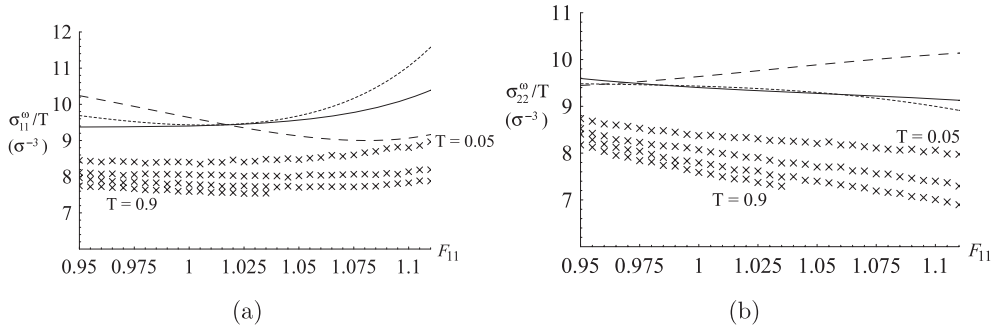

Figure 3. Comparison of the temperature-dependent (a) on-axis component $(\sigma_\omega)_{11}$ and (b) off-axis components $(\sigma_\omega)_{22} = (\sigma_\omega)_{33}$ of the Cauchy stress tensor for uniaxial deformation versus the stretch F_{11}. Shown are predictions from the QH (solid line), MLH (short dashes), and LH (long dashes) models versus the MD (crosses) results.

onset of instability as a function of strain and temperature with these critical values where discontinuities in the stress tensor are first observed. The initial instabilities correspond to localized defects in the solid and are dependent on the initial conditions of the simulation. At slightly larger critical strains or temperatures, we find that no initial conditions produce a stable solid. The critical strains and temperatures may be compared with predictions using any of the various stability criteria for a stressed solid. An upper bound on these critical values is found using the commonly employed Legendre–Hadamard condition [35, 36], a long-wavelength elastic measure of the stability. We may also equate a short-wavelength, or phonon, instability with the strain and temperature at which the QH or LH dynamical matrices no longer have real eigenvalues. A zero or imaginary eigenvalue corresponds to a localized deformation whose amplitude grows without energy penalty or without bound, respectively. This failure of the harmonic models is sensitively dependent on the model and range of potential, and it has not been previously pointed out as a limitation of the harmonic models.

In figure 3(a) we compare the MD data for a variety of temperatures with the harmonic predictions for the 11 component of the temperature-dependent part of the Cauchy stress σ_ω. We have subtracted the CB stress tensor from the measured MD virial stress in order to make a comparison with the predicted temperature-dependent contribution to the stress tensor, σ_ω. We then scale this tensor by temperature so that the data at different temperatures would fall on the same curve if the harmonic approximation were exact. That collapse to a single curve is not observed is indicative of the degree of anharmonicity in the system increasing with temperature and strain. Interestingly, none of the harmonic models reproduces the simulation data well even at low temperatures using this criterion. However, the scaling by temperature effectively reduces this contribution to the stress tensor at small temperatures so that the overall error between simulation and prediction remains small. The error between the data and the harmonic predictions is roughly similar for all three models, but the QH and MLH models clearly match the first derivative of the data more accurately than the LH model does. We see similar results for the off-axis stress in the uniaxial case (figure 3(b)) and for the equibiaxial case. Interestingly, all three harmonic models perform more or less equally well for isotropic deformation, as seen in figure 4. Overall, it is seen that one must consider the performance of the models under anisotropic deformation in order to completely describe the relative strengths of each approximation.

To further characterize the accuracy of the LH and MLH approximations, we consider the predictions of each model for the elastic stability limits of the solid. We employ a Legendre–

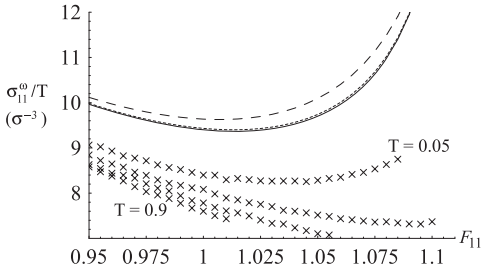

Figure 4. Comparison of the temperature-dependent diagonal component of the Cauchy stress $(\sigma_\omega)_{11} = (\sigma_\omega)_{22} = (\sigma_\omega)_{33}$ for isotropic stretch. Shown are predictions from the QH (solid line), MLH (short dashes), and LH (long dashes) models versus the MD (crosses) results.

Hadamard condition [35] to ascertain the large-scale incremental stability of the lattice, namely

$$\mathbb{B}_{iJkL} a_i N_J a_k N_L > 0 \qquad \forall a_i, N_J. \tag{12}$$

Here $\mathbb{B}$ is the so-called first elasticity tensor

$$\mathbb{B} = \frac{\partial \mathsf{P}}{\partial \mathsf{F}} = \frac{\partial^2 \mathcal{F}}{\partial \mathsf{F} \partial \mathsf{F}}. \tag{13}$$

Physically speaking, condition (12) can be interpreted as a requirement that small-amplitude plane wave solutions to the equation of motion linearized about the deformed configuration have positive, real frequencies; or in other terms, it requires that the deformed configuration is such that the equilibrium equation $\frac{\partial}{\partial \mathbf{X}} \cdot \mathsf{P} = \mathbf{0}$ is still elliptic [37, 38]. In the former interpretation, **N** is the propagation direction and **a** is the polarization vector. We find the eigenvalues of the acoustic tensor

$$\mathbf{A}_{ik}(\mathbf{N}) = \mathbb{B}_{iJkL} N_J N_L \tag{14}$$

for all **N** for a given deformation and temperature. If the minimum eigenvalue is non-positive the state is considered unstable. To follow the locus of stability points in (F, T) we start by finding the critical deformation F along the zero temperature curve, i.e. for $\mathbb{B} = \mathbb{B}_{\mathrm{CB}}$, and then index the one-parameter deformation gradient F and find the critical temperature for this deformation.

In figure 5 we show the predictions of the LH and MLH models for the long-wavelength elastic stability limits. Both models predict the same trends as the MD data, but the estimations of the MLH model for the maximum stable stretch at a given temperature are considerably smaller than those of the LH model. For each model, the failure mode is shear at low temperatures, while at higher temperatures the stability limit is governed by tensile failure. The critical strain for shear failure increases with increasing temperature while the tensile failure modes have a decreasing critical strain with increasing temperature. The shear failure regime is in essence the Born stability criterion for the vanishing shear modulus $C_{1212} = 0$ [39] except that additional finite-strain and temperature-dependent effects on the elastic moduli are included in the calculations. As temperature increases, the vibrational contribution of the harmonic models to the elastic moduli increases and eventually becomes the dominant factor in determining the stability locus. The transition temperature or strain from shear to tensile failure is consequently different for each of the harmonic approximations. The MLH model more accurately models the elastic moduli as a function of temperature and strain, and this accuracy is seen here to produce a better estimate of the onset of instability in the crystal, at least at low T. Neither estimate is very accurate at high T, however, indicating that a more localized measure for the onset of stability may be appropriate. This is not completely surprising since the short-wavelength modes become unstable at smaller strains than the longer wavelength

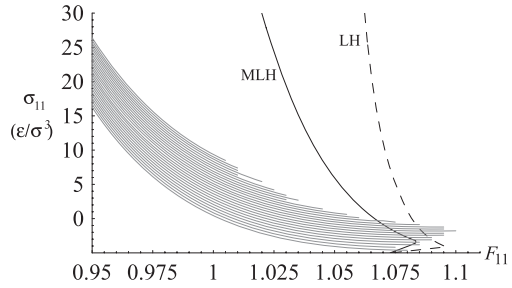

Figure 5. Comparison of the locus of instabilities seen in MD simulation against the long-wavelength elastic predictions for the onset of instability using the LH (long dashes) and MLH (solid) models for isotropic deformation.

modes in general. These data indicate that the most accurate stability measure may need to be based on the complete vibrational spectrum and not just the long-wavelength elastic properties. However, the MLH model is clearly seen to provide a better estimate than the LH model.

4. Discussion

It has been shown that all three harmonic models can be used to provide a reasonably-accurate constitutive model for the multiscale modeling of Lennard-Jones crystals using coupled MD–FEM simulations. Indeed, up to temperatures approaching the melt temperature, all three harmonic models can be said to be sufficiently accurate over a wide range of strains to closely follow the Cauchy stress tensor as determined from the MD simulation data. A critical examination of the temperature-dependent terms in the Cauchy stress tensor reveals that all three harmonic approximations have similar absolute errors between their predictions and the actual values seen from the MD simulations. At low temperatures, this error is small relative to the CB contribution to the stress, and at high temperatures the differences in the various harmonic approximations lead to different over-and under-estimations relative to the MD data. From this point of view, the LH model is insufficient to capture trends that depend on the elastic moduli or the strain derivatives of the stress tensor. The MLH and QH models do capture these trends, and the MLH is considerably less computationally expensive than the QH model. Of the deformation states studied, the LH model performs worst for uniaxial deformation and best for isotropic deformation. On the other hand, the MLH and QH models perform similarly for all the deformation states investigated. The more accurate approximation of the elastic moduli is also reflected in the ability of the MLH model to predict the onset of instability more accurately than the LH model.

The tremendous decrease in computer time gained with the LH and MLH models strongly argue against using the QH model in a multiscale simulation where the stress tensor is evaluated repeatedly for different local deformation states. Similarly, the MLH model is seen to be more accurate than the LH model, yet the first-order correction incurs only a modest additional computational cost. Consequently, the results shown here suggest that adoption of the MLH model would lead to some increase in the accuracy of current multiscale methods that use the LH model.

In this work and in many MD–FEM multiscale approaches, the atomistic-continuum correspondence is defined using the CB hypothesis. This CB rule has been shown to adequately treat dynamic effects such as strain rate, as seen, for instance, in multiscale studies of brittle fracture [40, 41]. Likewise, the CB hypothesis has been shown to remain useful down to even

subcontinuum length scales in carbon nanotubes [42]. Yet for systems containing surfaces, interfaces, defects, or dislocations, the CB rule is of limited utility even though the harmonic approximations may still be used to characterize the vibrational properties of the systems. Recent extensions of the quasicontinuum method have introduced methods to describe the continuum energetics using the so-called energy-based [43] and force-based formulations [44]. These methods define coarse-grained continuum energetics in terms of representative atomic configurations which need not be homogeneous, but their extension to nonzero temperatures remains ongoing. Consequently, this work here will be useful in characterizing a broad range of systems free of defects, dislocations, and interfaces, but its extension to more general systems remains a subject of ongoing investigation.

Finally, we note that investigations similar to those described here should be carried out for additional potentials, such as the embedded atom method (EAM) potentials. The Lennard-Jones potential used here is known to have smaller anharmonic effects than the EAM potentials. Similar critical investigations of the detailed dependence of the stress tensor on the deformation state for more anharmonic potentials can provide important indications of the robustness of these results and their general applicability to current multiscale efforts.

Acknowledgments

This work was funded by the Engineering Science Research Foundation at Sandia National Laboratories. This support is gratefully acknowledged. Sandia is a multiprogram laboratory operated by Sandia Corporation, a Lockheed Martin Company, for the United States Department of Energy under contract DE-ACO4-94AL85000.

Appendix. Dynamical matrices and their derivatives

Following section 2, we consider a static homogeneous deformation F with dynamic displacements $\{\mathbf{u}^\alpha\}$ about the deformed configuration. We use Greek indices to label atoms, dynamical matrices, or frequencies and reserve Arabic indices to label components (lowercase for current quantities and uppercase for referential). In component notation, the deformation gradient is

$$\mathsf{F}_{iJ} = \frac{\partial x_i}{\partial X_J} \tag{A.1}$$

where $\mathbf{e}_k$ and $\mathbf{E}_L$ are Euclidean basis vectors. Given

$$(r^\alpha)^2 = \mathbf{R}^\alpha \mathbf{C} \mathbf{R}^\alpha, \qquad \mathbf{C} \equiv \mathsf{F}^{\mathrm{T}}\mathsf{F} \tag{A.2}$$

and the pair potential ϕ, the derivatives of the frequencies with respect to the deformation can be calculated in a straightforward but tedious fashion.

With the restriction to pair potentials $\phi(r)$, the force constant matrix $\mathbf{D}^\alpha$ becomes

$$\mathbf{D}^\alpha = \delta^{\alpha 0} \sum_\gamma \frac{\partial^2 \phi}{\partial \mathbf{u}^\gamma \partial \mathbf{u}^0} - \frac{\partial^2 \phi}{\partial \mathbf{u}^\alpha \partial \mathbf{u}^0}. \tag{A.3}$$

The second derivatives in component notation are

$$\left.\frac{\partial^2 \phi}{\partial u_i^\alpha \partial u_j^0}\right|_{\mathbf{u}=0} = g(r^\alpha)\delta_{ij} + 2f(r^\alpha) r_i^\alpha r_j^\alpha \tag{A.4}$$

where $g(r) = r^{-1}\phi'(r)$ and $f(r) = r^{-2}(\phi''(r) - r^{-1}\phi'(r))$. In the QH model, we note that

$$\prod_\lambda \omega_{\mathbf{K}\lambda}^2 = \det D_{\mathrm{QH}}(\mathbf{K}). \tag{A.5}$$

Consequently, $\mathcal{F}$ can be written as a sum of determinants of the N dynamical matrices

$$\mathcal{F} = \Phi(\mathsf{F}) + \frac{k_B T}{2} \sum_{\mathbf{K}} \ln \det D_{\mathrm{QH}}(\mathbf{K}). \tag{A.6}$$

Likewise, within the LH model one has that

$$\prod_{\gamma} \omega_{\gamma}^2 = \det D_{\mathrm{LH}}. \tag{A.7}$$

The free energy becomes

$$\mathcal{F} = \Phi(\mathsf{F}) + \frac{k_B T}{2} \sum_{\alpha} \ln \det D_{\mathrm{LH}} \tag{A.8}$$

which may also be used to write down $\mathcal{F}$. Returning to the generic label γ for the different dynamical matrices, both models yield a free energy of the form

$$\mathcal{F} = \Phi(\mathsf{F}) + \frac{k_B T}{2} \sum_{\gamma} \ln \det D^{\gamma}. \tag{A.9}$$

As described in section 2, the MLH model is implemented as a single correction term applied to the Helmholtz free energy obtained within the LH approximation.

The determination of the temperature-dependent terms in the first Piola–Kirchoff stress in the QH or LH models thus reduces to determining the derivatives of the determinant with respect to the deformation gradient. For the MLH model, one supplements this with the derivatives of the force constants with respect to the strain. We note here that first-order perturbation theory may be used to write these eigenvalue derivatives in terms of the eigenvectors and the derivative of the dynamical matrix with respect to F. We prefer to calculate the derivatives directly from determinants of the dynamical matrices. Our approach offers considerable ease in implementing the second derivatives using symbolic algebra on the computer, and perhaps more importantly, subtleties about the treatment of degenerate frequencies do not arise. We calculate the derivatives of the determinant using the chain rule. In coordinate notation,

$$\det D^{\gamma} = D^{\gamma}_{1j} \mathsf{c}_{1j} = D^{\gamma}_{2j} \mathsf{c}_{2j} = D^{\gamma}_{1j} \mathsf{c}_{3j} \tag{A.10}$$

where summation over repeated variable indices is implied and c_{ij} is the the ij component of the adjugate of D^{γ}, i.e. the cofactor of D^{γ}_{ij}. With this result, Jacobi's formula gives us the necessary derivative

$$\frac{\partial \det D^{\gamma}}{\partial F_{kL}} = \frac{\partial D^{\gamma}_{ij}}{\partial F_{kL}} \mathsf{c}_{ij}. \tag{A.11}$$

The derivative of the QH dynamical matrix is given by

$$\frac{\partial D_{\mathrm{QH}}(\mathbf{K})}{\partial \mathsf{F}} = \sum_{\alpha} \frac{\partial D^{\alpha}}{\partial \mathsf{F}} \mathrm{e}^{-\mathrm{i}\mathbf{K}\cdot\mathbf{R}^{\alpha}}. \tag{A.12}$$

The derivatives of the LH dynamical matrix follow simply from equation (9) and the chain rule. When specialized to pair potentials, the derivative of D^{γ} is calculated from equations (A.3) and (A.4)

$$\frac{\partial D^{\alpha}_{ij}}{\partial F_{kL}} = \left(\frac{g'(r)}{2r} \delta_{ij} + \frac{f'(r)}{r} r_i r_j \right) R_P R_Q \frac{\partial C_{PQ}}{\partial F_{kL}} + f(r)(\delta_{ik} r_j R_L + \delta_{jk} r_i R_L). \tag{A.13}$$

The remaining required derivative above is given by

$$\frac{\partial C_{PQ}}{\partial F_{kL}} = (\delta_{PL} F_{kQ} + F_{kP} \delta_{QL}). \tag{A.14}$$

The temperature-dependent terms of the first Piola–Kirchoff stress become

$$V_0\,\mathsf{P}_\omega = \frac{k_\mathrm{B}T}{2}\sum_\gamma (\det D^\gamma)^{-1}\frac{\partial \det D^\gamma}{\partial \mathsf{F}}. \tag{A.15}$$

With this expression, the required components of the Cauchy stress tensor may be evaluated, too.

The elastic moduli are also now obtainable, although they involve considerably more computation in the QH approximation. Given the additive decomposition of the free energy $\mathcal{F}$, we obtain a similar one for the moduli

$$\mathbb{B} \equiv \frac{\partial \mathsf{P}}{\partial \mathsf{F}} = \mathbb{B}_\mathrm{CB} + \mathbb{B}_\omega. \tag{A.16}$$

We compute the CB contribution to the modulus

$$V_0(\mathbb{B}_\mathrm{CB})_{iJkL} = \delta_{ik}\frac{\partial \Phi}{\partial C_{JL}}\bigg|_{\mathbf{r}^\alpha} + 4\sum_\alpha \frac{\partial^2 \Phi}{\partial r^2 \partial r^2}\bigg|_{\mathbf{r}^\alpha} r_i R_J r_k R_L \tag{A.17}$$

by employing the fact that we are examining only pair potentials. The temperature-dependent tangent modulus is given by

$$V_0\mathbb{B}_\omega = \frac{k_\mathrm{B}T}{2}\sum_\gamma \left[-(\det D^\gamma)^{-2}\frac{\partial \det D^\gamma}{\partial \mathsf{F}}\otimes\frac{\partial \det D^\gamma}{\partial \mathsf{F}} + (\det D^\gamma)^{-1}\frac{\partial^2 \det D^\gamma}{\partial \mathsf{F}\partial \mathsf{F}}\right]. \tag{A.18}$$

The second derivative of the determinant is

$$\frac{\partial^2 \det D^\gamma}{\partial F_{lM}\partial F_{pQ}} = \frac{\partial D^\gamma_{ik}}{\partial F_{lM}\partial F_{pQ}}\mathsf{c}_{ik} + \frac{\partial D^\gamma_{ik}}{\partial F_{lM}}\frac{\partial \mathsf{c}_{ik}}{\partial F_{pQ}}, \tag{A.19}$$

which contains terms proportional to the second derivative of the dynamical matrices as well as terms containing the product of two first derivatives. The second derivative of the dynamical matrix is

$$\begin{aligned}\frac{\partial^2 D^\gamma_{ij}}{\partial F_{kL}\partial F_{mN}} = {} & (4r)^{-1}\left[\frac{\partial}{\partial r}\left(\frac{g'(r)}{r}\right)\delta_{ij} + \frac{\partial}{\partial r}\left(\frac{f'(r)}{r}\right)r_i r_j\right]R_P R_Q \frac{\partial C_{PQ}}{\partial F_{kL}} R_S R_T \frac{\partial C_{ST}}{\partial F_{mN}} \\ & + \left[\frac{g'(r)}{r}\delta_{ij} + \frac{f'(r)}{r}r_i r_j\right]R_L R_N \delta_{km} + \frac{f'(r)}{2r}(r_j R_N \delta_{im} + r_i R_N \delta_{jm})\frac{\partial r}{\partial F_{kL}} \\ & + \frac{f'(r)}{2r}(r_j R_L \delta_{ik} + r_i R_L \delta_{jk})\frac{\partial r}{\partial F_{mN}} + f(r)(R_L R_N \delta_{ik}\delta_{jm} + R_L R_M \delta_{jk}\delta_{im}).\end{aligned} \tag{A.20}$$

Within the QH approximation for a moderately sized system, this term is prohibitively expensive to evaluate using symbolic algebra programs.

References

[1] Barron T H K and Klein M L 1974 Perturbation theory of anharmonic crystals *Dynamical Properties of Solids* vol 1, ed G K Horton and A A Maradudin (Amsterdam: North-Holland)

[2] LeSar R, Najafabadi R and Srolovitz D J 1989 Finite-temperature defect properties from free-energy minimization *Phys. Rev. Lett.* **63** 624–7

[3] Rickman J M and Srolovitz D J 1993 A modified-local-harmonic model for solids *Phil. Mag.* A **67** 1081–94

[4] Najafabadi R and Srolovitz D J 1995 Evalution of the accuracy of the free-energy minimization method *Phys. Rev.* B **52** 9229

[5] Lacks D J and Shukla R C 1996 Molecular dynamics simulations of the effects of truncation of the Taylor expansion of the potential energy on the thermodynamic properties of a crystal *J. Chem. Phys.* **105** 4185

[6] Foiles S M 1994 Evaluation of harmonic methods for calculating the free energy of defects in solids *Phys. Rev.* B **49** 14930–8
[7] De Lorenzi G and Jacucci G 1986 Adequacy of lattice dynamics for high-temperature point-defect properties *Phys. Rev.* B **33** 1993
[8] Guido Della Valle R and Venuti E 1998 Quasiharmonic lattice dynamics and molecular dynamics calculations for the Lennard-Jones solids *Phys. Rev.* B **58** 206–12
[9] Dupuy L M, Tadmor E B, Miller R E and Phillips R 2005 Finite-temperature quasicontinuum: molecular dynamics without all the atoms *Phys. Rev. Lett.* **95** 060202
[10] Wagner G J and Liu W K 2003 Coupling of atomistics and continuum simulations using a bridging scale decomposition *J. Comput. Phys.* **190** 249–74
[11] Rudd R E and Broughton J Q 2005 Coarse-grained molecular dynamics: nonlinear finite elements and finite temperature *Phys. Rev.* B **72** 144104
[12] Born M 1940 On the stability of crystals I *Proc. Camb. Phil. Soc.* **36** 160–72
[13] Sutton A P 1989 Temperature-dependent interatomic forces *Phil. Mag.* A **60** 147–59
[14] Jiang H, Huang Y and Hwang K C 2005 A finite-temperature continuum theory based on interatomic potentials *J. Eng. Mat. Tech.* **127** 408
[15] Xiao S and Yang W 2006 Temperature-related Cauchy–Born rule for multiscale modeling of crystalline solids *Comput. Mater. Sci.* **37** 374–9
[16] Ericksen J L 1978 On the symmetry and stability of thermoelastic solids *Trans. ASME: J. Appl. Mech.* **45** 740–4
[17] Beatty M F 1987 Topics in finite elasticity: hyperelasticity of rubber, elastomers, and biological tissues—with examples *Appl. Mech. Rev.* **40** 1699–734
[18] Ball J M 2002 Some open problems in elasticity *Workshop on Geometry, Dynamics and Mechanics in Honour of the 60th Birthday of Jerrold E Marsden* ed P Newton, P Holmes and A Weinstein (Berlin: Springer) pp 3–59
[19] Marsden J E and Hughes T J R 1983 *Mathematical Foundations of Elasticity* (Englewood Cliffs, NJ: Prentice-Hall)
[20] Truesdell C and Noll W 2003 *The Non-Linear Field Theories of Mechanics* 3rd edn, ed S S Antman (Berlin: Springer)
[21] Ericksen J L 1986 Stable equilibrium-configurations of elastic crystals *Arch. Ration. Mech. Anal.* **94** 1–4
[22] Davini C 1986 Proposal for a continuum theory of defective crystals *Arch. Ration. Mech. Anal.* **96** 295–317
[23] Cermelli P and Sellers S 2000 Multi-phase equilibrium of crystalline solids *J. Mech. Phys. Solids* **48** 765–96
[24] Pitteri M 1990 Some problems in nonlinear elasticity of crystalline solids *Contin. Mech. Thermodyn.* **2** 99–117
[25] Fonseca I and Parry G 1992 Equilibrium configurations of defective crystals *Arch. Ration. Mech. Anal.* **120** 245–83
[26] E W and Ming P B 2007 Cauchy–Born rule and the stability of crystalline solids: static problems *Arch. Ration. Mech. Anal.* **183** 241–97
[27] Hill R and Milstein F 1977 Principles of stability analysis of ideal crystals *Phys. Rev.* B **15** 3087
[28] Morris J W Jr and Krenn C R 2000 The internal stability of an elastic solid *Phil. Mag.* A **80** 2827–40
[29] Zimmerman J 1999 Continuum and atomistic modeling of dislocation nucleation at crystal surface ledges *PhD Thesis* Stanford University
[30] Allen M P and Tildesley D J 1989 *Computer Simulation of Liquids* (Oxford: Clarendon)
[31] Wallace D C 1972 *Thermodynamics of Crystals* (Mineola, NY: Dover)
[32] Morris J R and Song X 2002 The melting lines of model systems calculated from coexistence simulations *J. Chem. Phys.* **116** 9352
[33] Jin Z H, Gumbsch P, Lu K and Ma E 2001 Melting mechanisms at the limit of superheating *Phys. Rev. Lett.* **87** 055703
[34] Gomez L, Gazza C, Dacharry H, Penaranda L and Dobry A 2005 Pressure dependence of the melting mechanism at the limit of overheating in Lennard-Jones crystals *Phys. Rev.* B **71** 134106
[35] Truesdell C and Noll W 1965 The non-linear field theories of mechanics *Encyclopedia of Physics* vol 3, ed S Flugge (Berlin: Springer)
[36] Chen Y-C 1991 On strong ellipticity and the Legendre–Hadamard condition *Arch. Ration. Mech. Anal.* **113** 165–75
[37] Hill R 1962 Acceleration waves in solids *J. Mech. Phys. Solids* **10** 1–16
[38] Fago M, Hayes R L, Carter E A and Ortiz M 2004 Density-functional-theory-based local quasicontinuum method: prediction of dislocation nucleation *Phys. Rev.* B **70** 100102R
[39] Born M 1939 Thermodynamics of crystals and melting *J. Chem. Phys.* **7** 591
[40] Miller R, Tadmor E B, Phillips R and Ortiz M 1998 Quasicontinuum simulation of fracture at the atomic scale *Modelling Simul. Mater. Sci. Eng.* **6** 607–38

[41] Park H S, Karpov E G, Liu W K and Klein P A 2005 The bridging scale for two-dimensional atomistic/continuum coupling *Phil. Mag.* **85** 79–113
[42] Arroyo M and Belytschko T 2004 Finite crystal elasticity of carbon nanotubes based on the exponential Cauchy–Born rule *Phys. Rev.* B **69** 115415
[43] Miller R E and Tadmor E B 2002 The quasicontinuum method: overview, applications and current directions *J. Comput.-Aided Mat. Des.* **9** 203–39
[44] Knap J and Ortiz M J 2001 An analysis of the quasicontinuum method *J. Mech. Phys. Solids.* **49** 1899